JOURNAL OF CATALYSIS **163,** 95–105 (1996)
ARTICLE NO. 0308

Electrochemical Oxidation of Methanol over a Silver Electrode Deposited on Yttria-Stabilized Zirconia Electrolyte

Jin Ki Hong, In-Hwan Oh,* Seong-Ahn Hong,* and Wha Young Lee[1]

*Department of Chemical Engineering, Seoul National University, Shinlim-dong, Kwanak-ku, Seoul 151-742, Korea; and *Division of Chemical Engineering, Korea Institute of Science and Technology, Hawolkok-dong, Seongbuk-ku, Seoul 136-791, Korea*

Received February 12, 1996; revised April 29, 1996; accepted May 28, 1996

A solid electrolyte catalytic reactor was used to investigate the change in catalytic activity of the electrode upon conduction of O^{2-} ions through the electrolyte. The reactor consisted of an yttria-stabilized zirconia electrolyte disk on which a thin film of the Ag electrode was deposited. As the catalyst potential was applied below the open circuit potential or, equivalently, as O^{2-} ions were electrochemically removed from the Ag catalyst electrode to the counter electrode through the solid electrolyte, its influence on the O_2 exchange reaction in He–O_2 flow and CH_3OH oxidation to HCHO and CO_2 in He–O_2–CH_3OH flow was investigated. It was found from the O_2 exchange reaction study that slow diffusion of adsorbed oxygen to the catalyst–electrolyte–gas three-phase boundary, where charge transfer took place, caused a limiting current. In CH_3OH oxidation, a lowered open circuit potential was observed when CH_3OH was added to the He–O_2 flow. Lowering the catalyst potential below this new open circuit potential was found to cause a reversible, somewhat nonfaradaic increase in the rate of CO_2 formation, but had little effect on the rate of HCHO formation. Based on the rate equations, this behavior was interpreted in terms of an activated surface reaction between adsorbed species due to the change in the catalyst work function with changing catalyst potential.

INTRODUCTION

Heterogeneous catalysis and electrochemistry were not interrelated until ion conducting inorganic materials, i.e., solid electrolytes, were developed. However, the use of cells of the type

$$\text{Gaseous reactants, W} \mid \text{solid electrolyte} \mid \text{C, air } (O_2), \quad [1]$$

where W and C respectively denote the working and counter electrodes, which are usually metal films, have enabled us to combine these two subjects. For example, a Ag electrode deposited on 8 mol% yttria-stabilized zirconia (YSZ) electrolyte, abbreviated Ag/YSZ, has catalytic activity as well as electrochemical characteristics based on O^{2-} ion conduction. The counter electrode exposed to oxygen catalyzes the oxygen exchange reaction,

$$O_{2(g)} + 4e^- \Longleftrightarrow 2O^{2-}, \quad [2]$$

and serves to supply (or remove) O^{2-} ions to (or from) the working electrode through the electrolyte.

The open circuit potential (OCP), which measures the equilibrium potential of the working electrode with respect to the reference electrode, can be determined from gas activities on both electrodes. When the oxygen exchange reaction shown in Eq. [2] is dominant on the electrode and thermodynamic equilibrium is established between the oxygen in the gas phase and the adsorbed oxygen on the electrode ($a_0^2 = P_{O_2}$), the OCP can be calculated from the Nernst equation (1),

$$V_{WR}^{\circ} = \frac{RT}{4F} \ln \frac{P_{O_2,W}}{P_{O_2,R}}. \quad [3]$$

Here, V_{WR}° is the OCP between the working and the reference electrode, R is the gas constant, T is the absolute temperature, F is Faraday's constant, and $P_{O_2,W}$ and $P_{O_2,R}$ are the oxygen pressure in the working electrode side and that in the reference electrode side, respectively.

In general, however, when other gaseous reactants in addition to oxygen are present in the working electrode side and the cell is under an open circuit condition, the working electrode acts as a normal catalyst for gaseous reactants and the OCP shifts to a new value which is different from the OCP of the oxygen exchange reaction. This new value might be a mixed potential of two or more redox processes of gaseous reactants on the electrode surface (2). If the circuit is closed and a potentiostat is used to apply the catalyst potential above the OCP (anodic overpotential, $\Delta V_{WR} = V_{WR} - V_{WR}^{\circ} > 0$, where V_{WR} is the catalyst potential with respect to the reference electrode and V_{WR}° is V_{WR} under open circuit condition), then the resulting current measured will be positive ($I > 0$, anodic current) and therefore, O^{2-} ions are transferred from the counter electrode to the working electrode (catalyst) through the electrolyte at a rate of $I/(2F)$. Similarly, at the cathodic overpotential ($\Delta V_{WR} < 0$)

[1] To whom correspondence should be addressed.

0021-9517/96 $18.00

where cathodic current ($I < 0$) flows, O^{2-} ions are pumped from the working electrode to the counter electrode.

Vayenas *et al*. (3–5) studied catalytic reactions over metal electrodes deposited on a solid electrolyte. They demonstrated a distinct, reversible change in catalytic activity of the electrode by ion conduction through the electrolyte when the catalyst potential was changed from its open circuit value. O^{2-} ions supplied to or from the catalyst through the electrolyte could cause reactions of many chemisorbed molecules in addition to electrocatalytic reactions, i.e., net charge transfer reactions where Faraday's law was valid. They referred to such a change in catalytic rate, which was not limited by Faraday's law, with variation of the catalyst potential as the nonfaradaic electrochemical modification of catalytic activity (NEMCA) effect. This phenomenon has been known not to be restricted to any particular catalyst or catalytic reaction, thereby presenting new theoretical and experimental areas in catalytic enhancement. Polarization between the working electrode and the electrolyte, $e\Delta V_{WR}$, where e is the charge of an electron and ΔV_{WR} is the overpotential as defined above, affects the concentration of O^- or O^{2-} ions on the surface of the working electrode. The presence of O^- or O^{2-} ions, different from adsorbed oxygen, was confirmed by the XPS, study (6). The spillover of these ions on the electrode develops a dipole which leads to the change in work function, $\Delta e\Phi$, of the electrode as shown in the following relationship (3–7):

$$e\Delta V_{WR} = \Delta e\Phi. \quad [4]$$

This equation implies that the work function of the electrode can be considered one of the variables, like reaction temperature or reactant concentrations. For example, for first-order Eley–Rideal type reactions, the rates of catalytic reactions, r, depend exponentially on the catalyst potential, V_{WR}, according to the relation

$$\ln\frac{r}{r_0} = \alpha F(V_{WR} - V^*_{WR})/RT, \quad [5]$$

where r_0 is the normal (i.e., under open circuit) catalytic rate, and α and V^*_{WR} are reaction- and catalyst-specific constants (5).

The NEMCA effect in the case of CH_3OH oxidation on Pt has been intensively studied by Vayenas and Neophytides (7). They found that catalytic activity and selectivity of polycrystalline Pt for the oxidation of CH_3OH to HCHO and CO_2 can be dramatically and reversibly affected when O^{2-} ions are electrochemically pumped to or from the Pt catalyst surface. They interpreted the observed behavior by taking the change in catalyst work function with changing catalyst potential and the concomitant changes in the strength of chemisorptive bonds into account.

Ag has a high catalytic activity and is relatively inexpensive as a catalyst compared with other noble metals. Since CH_3OH oxidation over Ag as a catalyst has been important in industry, it has drawn many researchers' interest. High selectivity for HCHO has been reported under CH_3OH-rich conditions (8). Studies on the adsorption of O_2 and CH_3OH on Ag and their reaction characteristics have been carried out (9–11). Robb and Harriott (12) suggested a Langmuir–Hinshelwood model for the reaction mechanism, whereas the fractional order with respect to CH_3OH and O_2 was shown to fit the rate equation (13).

Although the NEMCA effect has been studied for many catalytic reactions on Pt, Pd, and Ag (3), CH_3OH oxidation over Ag with the NEMCA effect has not yet been studied. In this study, therefore, O_2 adsorption and CH_3OH oxidation over Ag/YSZ under open circuit and polarization conditions are investigated to determine the NEMCA effect on reaction rates. Reaction mechanisms and rate equations under open circuit conditions are also proposed to support our explanation. Since the morphology and characteristics of the Ag catalyst were irreversibly changed at high anodic overpotentials (14), only the effect of cathodic overpotential on the reaction rates is discussed in this study.

EXPERIMENTAL

Ag/YSZ Preparation

The YSZ disk was prepared by pressing 8 mol% YSZ powders (Tosoh, TZ-8Y) with a pelletizer at a pressure of 5 MPa. Isostatic pressing at 100 MPa was then applied to this disk. A YSZ solid electrolyte with high ionic conductivity and mechanical strength, of diameter 24 mm and thickness 1.0 mm, was obtained by sintering at 1450°C. Its surface was polished with a SiC paper, cleaned in ethanol solution, and dried. A Ag paste (Fujikura Kasei, Dotite D-500) was printed on the YSZ disk through a silk screen and then sintered at 650°C to obtain a porous thin film with a thickness of about 10 μm. SEM (Jeol, JSM-35) images show that the Ag electrode, working as a catalyst, consists of a fine network of regular texture, as shown in Fig. 1. It was assumed that the resistance to diffusion of gaseous oxygen through the pores in the Ag electrode was negligible due to its relatively large pore size. Surface impurity was checked by AES (Perkin–Elmer, ϕ 670). Only trace amounts of Cl were detected and the Ag surface was found to be fairly clean. On the opposite side of the Ag electrode, counter and reference electrodes were deposited in the same as described above. The area of the counter electrode was three times that of the working electrode and the reference electrode was kept as small as possible to minimize the internal resistance.

Apparatus and Methods

The YSZ disk and one end of the alumina tube, through which reactants flow in and out, were sealed with glass powder (Nippon Electric Glass, GA-4/325). Reactants were

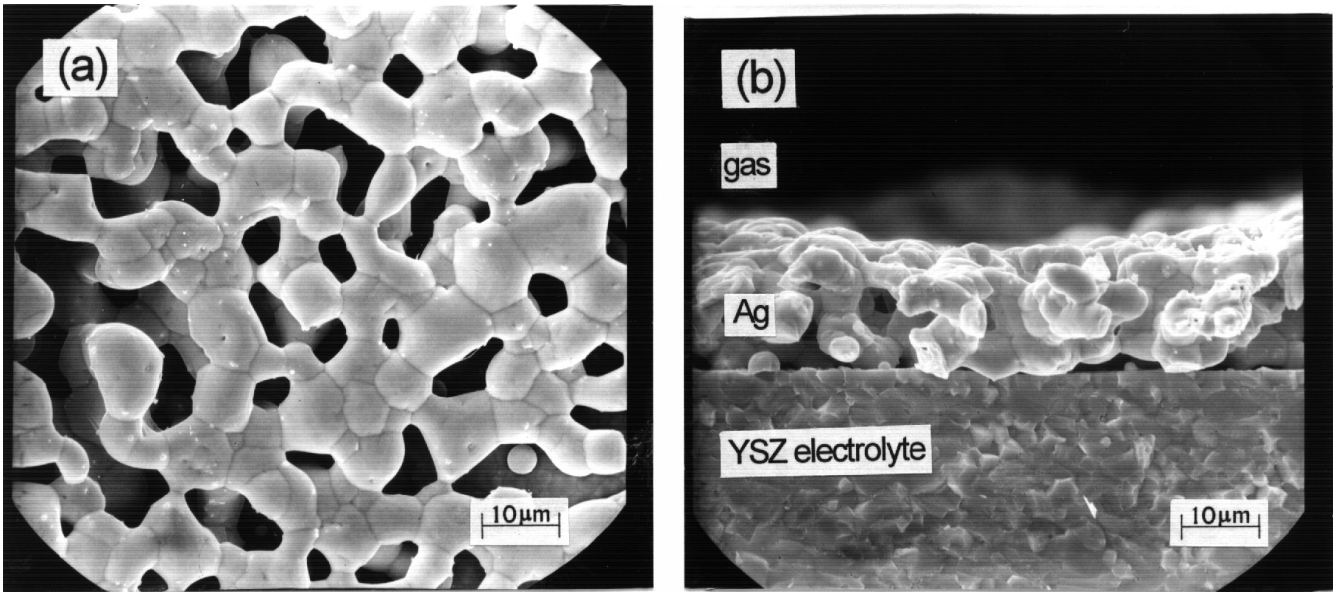

FIG. 1. Scanning electron micrograph of the surface of the Ag electrode (a) and of the cross-section perpendicular to the Ag electrode–YSZ electrolyte interface (b).

supplied to the Ag electrode while the opposite side, consisting of the counter and reference electrodes, was exposed to ambient air. The solid electrolyte catalytic reactor, as shown in Fig. 2, had an internal volume of 62 cm^3 and was assumed to be well mixed (CSTR) over the range of flow rates studied. The reactor temperature, 500°C, was measured by a CA-type thermocouple placed near the reactor and controlled to within ± 1°C by a PID controller. The flow rate of the reactants, He and O_2, was controlled by a mass flow controller (Sierra Instruments, Side Trak III) and checked by a digital flowmeter (Humonics, Optiflow 520). The flow rate through the reactor was also compared with that through the bypass line to check for leakage in the reactor. CH_3OH was supplied at a constant flow rate by a syringe pump (Sage Instruments, 341B), and reactants were mixed in the mixing chamber before entering the reactor. The flow line was heated above 125°C to prevent the condensation of reactants and products. Products were analyzed by on-line gas chromatography (Yanaco, G-1800, TCD type, column material: Porapak T and Carbosphere) and on-line mass spectroscopy (Anelva, AGA-360) at the same time.

Open circuit potential and polarization curves were obtained using a potentiostat (EG&G, 273A) which was manipulated by a personal computer. With the current interruption method, the internal resistance (IR) of the YSZ electrolyte or the resistance between the catalyst and the reference electrode could be compensated; hence the IR-free catalyst potential V_{WR} could be determined. All the polarization experiments were conducted after the open circuit potential reached a stable value. The current during the

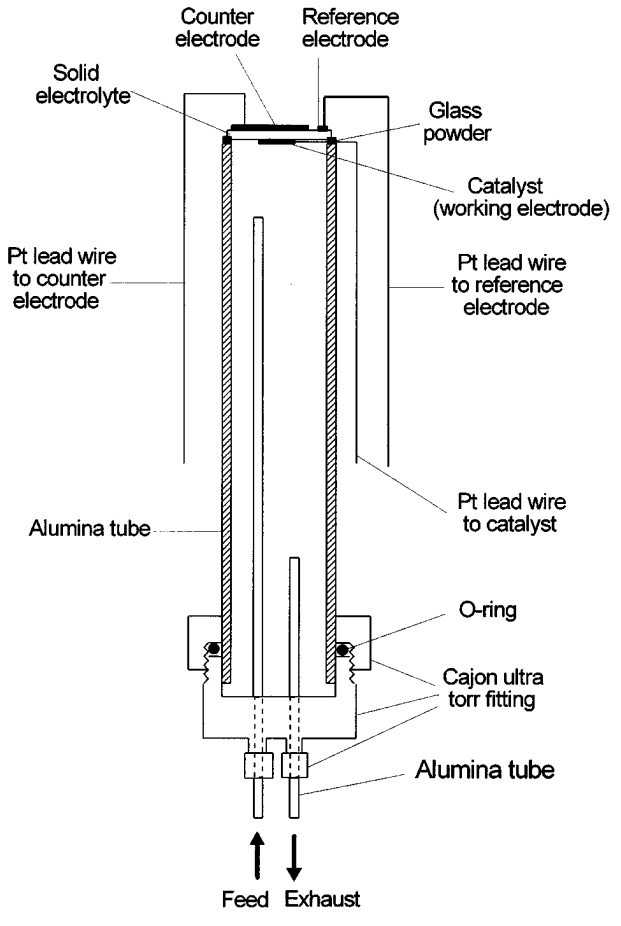

FIG. 2. Schematic diagram of a solid electrolyte catalytic reactor.

slow potential scan (0.1 mV/sec) showed nearly the same results as the current obtained at constant potentials (potentiostatic mode), indicating that results obtained at the low scan rate could be considered equivalent to steady state results.

RESULTS AND DISCUSSION

O_2 Exchange Reaction

The OCP between the catalyst (working electrode) and the reference electrode is determined from the difference of chemical potentials on both electrodes as

$$V^{\circ}_{WR} = \frac{1}{4F}[\mu_{O_2(M)catalyst} - \mu_{O_2(M)reference}], \quad [6]$$

where $\mu_{O_2(M)}$ is the chemical potential of oxygen adsorbed on the metal electrode. This equation is based on the assumption that YSZ conducts only O^{2-} ions and that the oxygen exchange reaction is dominant on the electrode. The chemical potential of oxygen adsorbed on the reference electrode ($\mu_{O_2(M)reference}$) which is exposed to air ($P_{O_2} = 0.21$ atm) is written as

$$\mu_{O_2(M)reference} = \mu^{\circ}_{O_2(g)} + RT \ln(0.21), \quad [7]$$

where $\mu^{\circ}_{O_2(g)}$ is the standard chemical potential of oxygen at temperature T. In the same way, the chemical potential of oxygen adsorbed on the catalyst electrode is

$$\mu_{O_2(M)catalyst} = \mu^{\circ}_{O_2(g)} + RT \ln(a_0^2), \quad [8]$$

where a_0 is the oxygen activity on the catalyst electrode. Thus, it is the oxygen activity on the electrode that determines the OCP. When thermodynamic equilibrium is established between oxygen in the gas phase and that adsorbed on the electrode ($a_0^2 = P_{O_2}$), substitution of Eq. [7] and Eq. [8] into Eq. [6] gives the following Nernst equation:

$$V^{\circ}_{WR} = \frac{RT}{4F} \ln \frac{P_{O_2}(atm)}{0.21}. \quad [9]$$

If ln in Eq. [9] is replaced with log, then the slope 2.3 $RT/4F$ is calculated to be 38.4 mV/decade at 500°C. If corrosion leading to the formation of surface oxides occurs on the electrode, the slope will increase (15).

The OCP measured in this study, with Ag exposed to air as a reference electrode, is almost the same as that calculated from Eq. [9], implying that no corrosion takes place under experimental conditions and that the oxygen exchange reaction is dominant on the electrode. The independent calculation from a thermodynamic program (16) and experimental data (17) of the thermodynamic equilibrium state of Ag exposed to oxygen also showed that no oxide could be formed on the Ag surface due to the strong reducibility of Ag. Hillary and Stoukides (18) also confirmed during their study on H_2 oxidation over Ag that the Ag electrode had a clean surface under open circuit conditions.

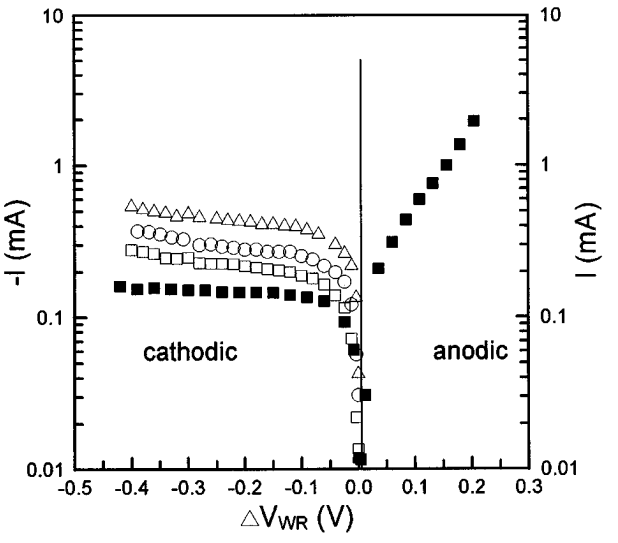

FIG. 3. Current–overpotential curves with P_{O_2}: 0.20 atm (△), 0.10 atm (○), 0.05 atm (□), and 0.02 atm (■). $T = 500$°C.

Figure 3 shows the current–overpotential curves at the scan rate of 0.1 mV/sec for four different oxygen pressures. It is seen that the anodic current curve at P_{O_2} of 0.02 atm followed Tafel behavior (19), indicating that the charge transfer is the limiting step in the anodic reaction of the oxygen ion ($O^{2-} \rightarrow O_{(a)} + 2e^-$). Anodic current curves at P_{O_2} higher than 0.02 atm revealed a remarkably steep increase in current with anodic overpotential, suggesting a structural change of the Ag electrode (14). Once the structure of the Ag electrode changed, it would affect further experiments. In this study, therefore, the anodic reaction of oxygen was performed only at P_{O_2} of 0.02 atm and further study of anodic reactions at P_{O_2} higher than 0.02 atm was not carried out to avoid any irreversible change of the Ag electrode.

Figure 3 also shows that the cathodic current reached a limiting value at high cathodic overpotential and that the absolute value of the limiting current increased with P_{O_2}. When the total flow rate increased at constant P_{O_2}, the cathodic current curve remained the same. These results strongly suggest that the limiting current resulted from the interfacial diffusion of adsorbed oxygen from adsorption sites to the electrode–electrolyte–gas three-phase boundary where charge transfer takes place, not from the slow diffusion of gaseous oxygen through the electrode pores or the low adsorption rate of oxygen on the working electrode.

In their recent paper, Wang and Nowick (20) claimed that the limiting current is observed when diffusion of gaseous oxygen through the electrode pore or adsorption rate on the electrode surface is so low that oxygen coverage is almost zero, and proposed the following relationship between

current I and oxygen coverage θ,

$$\theta/\theta_e = (|I_{lim}| - |I|)/|I_{lim}|, \quad [10]$$

where θ_e is the oxygen coverage in equilibrium and $|I_{lim}|$ is the absolute value of the limiting current. However, the assumption that the limiting current is observed at $\theta = 0$ cannot explain the observed dependence of limiting current on $P_{O_2}^{0.5}$.

We now propose a new equation to explain the relationship between the limiting current and P_{O_2} as shown in Fig. 3, assuming that the limiting current is proportional to the oxygen coverage and oxygen coverage is not affected at high cathodic overpotentials; i.e.,

$$|I_{lim}| \propto \theta_e. \quad [11]$$

If Langmuir adsorption is assumed, then

$$\frac{\theta_e}{1-\theta_e} = [K(T)P_{O_2}]^{0.5}, \quad [12]$$

where

$$K(T) = K_0 \exp(\Delta H_{ad}/kT). \quad [13]$$

Here, $K(T)$ is the adsorption equilibrium constant at the absolute temperature T, K_0 is the preexpontial factor, ΔH_{ad} is the adsorption head of oxygen, and k is the Boltzmann constant. It is well known that oxygen is adsorbed dissociatively on Ag and its equilibrium surface coverage on Ag is smaller than that on Pt. Surface coverage of oxygen on polycrystalline Ag film was reported to be 0.5 at 500°C and 1.6 atm P_{O_2} (21). From this fact, θ may be assumed to be much less than 0.5 for low P_{O_2} as in this study and a combination of Eqs. [11] and [12] gives

$$|I_{lim}| \propto [K(T)P_{O_2}]^{0.5}. \quad [14]$$

As $|I_{lim}|$ is proportional to θ_e, as suggested in Eq. [11], $|I_{lim}|$ is proportional to $P_{O_2}^{0.5}$. To confirm this hypothesis, the dependence of $|I_{lim}|$ on P_{O_2} was investigated, and the result is shown in Fig. 4. It is seen that the experimentally obtained slope, 0.53, was in fairly good agreement with the theoretical value of 0.5. Threfore, it may be concluded that the cathodic limiting current was proportional to $P_{O_2}^{0.5}$ and it resulted from the interfacial diffusion of adsorbed oxygen to the electrode–electrolyte–gas three-phase boundary.

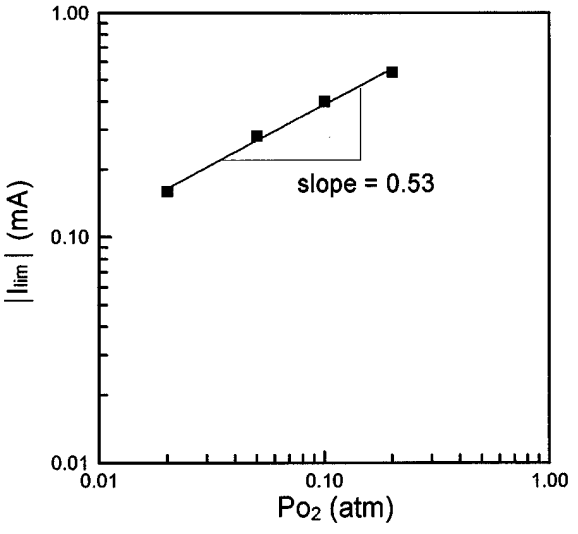

FIG. 4. Dependence of the limiting current, $|I_{lim}|$, on P_{O_2}.

OCP in He–O_2–CH_3OH Flow

When CH_3OH was added to He–O_2 flow, the OCPs at the various gas flows were measured to see the effect of the presence of CH_3OH on the reversible kinetic change; the results are summarized in Table 1. When only He gas flowed, the OCP measured was −102 mV. The P_{O_2} corresponding to this OCP estimated from the Nernst equation [9] is 4.6×10^{-4} atm, which might be explained by traces of oxygen contained in He gas. When CH_3OH (5 mol%) was added to He–O_2 (5 mol%) flow, a significant change in the OCP was observed from −24 to −735 mV. Measurement of P_{O_2} in the reactor by GC indicated that 18% of supplied oxygen had been consumed by the catalytic oxidation of CH_3OH for the He–O_2 (5 mol%)–CH_3OH (5 mol%) flow. However, independent calculation of P_{O_2} from the observed OCPs using the Nernst equation [9] showed that P_{O_2} for the He–O_2 (5 mol%)–CH_3OH (5 mol%) flow was lower than that for the He–O_2 (5 mol%) flow by several orders of magnitude. All of these results imply that the OCP in flow where CH_3OH is present cannot be determined by the oxygen exchange reaction alone. Vayenas (22) reported that the OCP was lowered by 100–200 mV when CO was introduced as a reactant. This change in the OCP was considered to result from the low surface coverage of oxygen by fast reaction on the surface of the electrode. However, since it is likely that the adsorption equilibrium of oxygen was not established in that case, i.e., $a_0^2 < P_{O_2}$, the other mechanism is needed to explain the effect of CH_3OH presence on the OCP change.

One way to explain this discrepancy between the experimental OCP and the estimated OCP is to consider other

TABLE 1

Open Circuit Potential for Various Inlet Gas Compositions ($T = 500$°C)

Inlet gas composition	Open circuit potential (mV)
He	−102
He + O_2 (5 mol%)	−24
He + O_2 (7 mol%) + CH_3OH (5 mol%)	−634
He + O_2 (5 mol%) + CH_3OH (5 mol%)	−735
He + O_2 (3 mol%) + CH_3OH (5 mol%)	−880
He + CH_3OH (5 mol%)	−1015

electrochemical reactions as well as an oxygen exchange reaction. Because products such as HCHO, CO_2, and H_2O are formed in He–O_2–CH_3OH flow on the Ag electrode, the following electrochemical reactions are possibly occurring:

$$CH_3OH + O^{2-} \Longleftrightarrow HCHO + H_2O + 2e^- \quad [15]$$

$$CH_3OH + 3O^{2-} \Longleftrightarrow CO_2 + 2H_2O + 6e^-. \quad [16]$$

Fuel cell type reactions can be written as follows when reactions [15] and [16] are proceeding anodically and the oxygen exchange reactions are proceeding cathodically:

$$CH_3OH + \tfrac{1}{2}O_2 \Longleftrightarrow HCHO + H_2O \quad [17]$$

$$CH_3OH + \tfrac{3}{2}O_2 \Longleftrightarrow CO_2 + 2H_2O. \quad [18]$$

The electromotive force, E^0, of a fuel cell type reaction can be determined theoretically (23) from the relation

$$E^0 = -\Delta G^0/nF, \quad [19]$$

where G^0 is the standard Gibbs free energy and n is the number of electrons involved in the reaction. E^0 is the electromotive force for the standard states of reactants and is generally found to be weakly dependent on reactant concentration. E^0 at 500°C obtained from thermodynamic data (17) for reactions [17] and [18] is 1081 and 1232 mV, respectively, as listed in Table 2. The OCPs for reactions [15] and [16] should be lower than that of the oxygen exchange reaction in E^0 values. Therefore, the OCP in He–O_2 (5 mol%)–CH_3OH (5 mol%) flow lies between that of the oxygen exchange reaction (−24 mV) and those of reactions [15] and [16]. The OCP in He–CH_3OH flow where O_2 is not present is seen to be close to those of reactions [15] and [16]. These results strongly suggest that the OCP in He–O_2–CH_3OH flow is a mixed potential established by reactions [15] and [16] as well as the oxygen exchange reaction. The mixed potential is the one determined by the kinetic equilibrium of possible electrochemical reactions (2, 24) and depends on the individual OCPs and the exchange current density of each reaction. The decrease in OCP by the addition of CH_3OH can be also explained from the surface science viewpoint. Depletion of negatively charged oxygen species by the catalytic oxidation of CH_3OH on the catalyst surface produces a positive change in the surface potential, i.e. a decrease in catalyst work function (25). The decrease in the catalyst work function increases the electrochemical potential of electrons in the catalyst, leading to the lowering of the OCP as represented in Eq. [4]. As shown in Table 1, as the inlet mole fraction of oxygen increases from 3 to 7 mol% in He–O_2–CH_3OH (5 mol%) flow, the OCP in terms of a mixed potential approaches that of the oxygen exchange reaction. After the supply of CH_3OH is stopped, the OCP returns to that of the oxygen exchange reaction, reversibly.

TABLE 2

Electromotive Force for Reactions [17] and [18] ($T = 500$°C)

Reaction	$-\Delta G^\circ$ (kJ/mol)	n	E° (mV)
[17] $CH_3OH + \frac{1}{2}O_2 \rightarrow HCHO + H_2O$	208.7	2	1081
[18] $CH_3OH + \frac{3}{2}O_2 \rightarrow CO_2 + 2H_2O$	713.1	6	1232

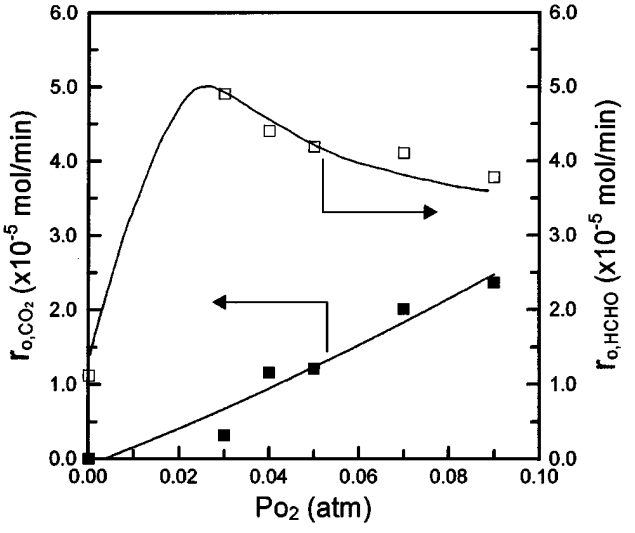

FIG. 5. Variation of r_{0,CO_2} (■) and $r_{0,HCHO}$ (□) with inlet P_{O_2} under open circuit condition. $T = 500$°C and inlet $P_{CH_3OH} = 0.05$ atm.

CH_3OH Oxidation under Open Circuit Conditions

To investigate the oxidation mechanism of CH_3OH to HCHO and CO_2 over the Ag catalyst, the formation rates of CO_2 and HCHO under open circuit conditions (r_{0,CO_2} and $r_{0,HCHO}$) were measured with changing inlet P_{O_2} at constant inlet P_{CH_3OH}. The result is shown in Fig. 5. When oxygen was absent, only the decomposition of CH_3OH proceeded, producing H_2, CH_4, CO, and HCHO. When oxygen was added, the main products were changed to HCHO, CO_2, and H_2O due to the CH_3OH oxidation. As inlet P_{O_2} increased r_{0,CO_2} increased steadily while $r_{0,HCHO}$ first increased and then decreased slightly. This result is consistent with Xinhe and Jingfa's study (10) that over a certain P_{O_2} where $r_{0,HCHO}$ reaches a maximum, the total oxidation increased with the increase in the surface oxygen coverage. In this study, the oxygen coverage where $r_{0,HCHO}$ is maximum lies between 0 and 0.03 atm of inlet P_{O_2}, suggesting that the surface reaction seems to limit the overall oxidation rate of CH_3OH.

Wachs and Madix proposed the following mechanism, assuming that HCHO is formed by the decomposition of CH_3OH and further oxidation of HCHO leads to total

oxidation (26):

$$\begin{array}{c} CH_3OH_{(g)} \\ \downarrow\uparrow \\ CH_3O_{(a)} \\ \downarrow\uparrow \\ HCHO_{(g)} \rightleftarrows HCHO_{(g)} \\ \downarrow \longleftarrow O_{(a)} \\ CO_{2(a)}, H_2O_{(a)} \\ \downarrow\uparrow \\ CO_{2(g)}, H_2O_{(g)} \end{array}$$

Subscripts (g) and (a) in the above mechanism represent the gas phase and the adsorbed phase, respectively. The surface species of oxygen on Ag has been known to be the dissociatively adsorbed atom. The methoxy group, an intermediate, on the polycrystalline Ag surface with preadsorbed oxygen was identified by the HREELS experiment (27). Decomposition of methoxide yields HCHO and H_2O.

As shown in Fig. 5 and mentioned earlier, r_{0,CO_2} increased steadily with inlet P_{O_2}. This observation suggests that the oxidation of surface HCHO to CO_2 may be a rate-limiting step. From Wachs and Madix's mechanism (26), the reaction steps may be written as

Step 1 $O_{2(g)} \Longleftrightarrow 2O_{(a)}$
Step 2 $CH_3OH_{(g)} \Longleftrightarrow HCHO_{(a)} + 2H_{(a)}$
Step 3 $HCHO_{(a)} \Longleftrightarrow HCHO_{(g)}$
Step 4 $HCHO_{(a)} + 2O_{(a)} \rightarrow CO_{2(a)} + H_2O_{(a)}$
Step 5 $CO_{2(a)} \Longleftrightarrow CO_{2(g)}$
Step 6 $H_2O_{(a)} \Longleftrightarrow H_2O_{(g)}$
Step 7 $2H_{(a)} + O_{(a)} \rightarrow H_2O_{(a)}$,

where Step 4 is assumed to be a rate-limiting step and Step 7 of the hydrogen oxidation is thought to be fast enough. The surface coverage of each species was also considered to be fairly low for the high reaction temperature in this study. From the elementary reaction steps, adsorption equilibrium can be expressed as follows:

Step 1 $k_1 P_{O_2} = k_1' \theta_0^2$
Step 2 $k_2 P_{CH_3OH} = k_2' \theta_{HCHO} \theta_H^2$
Step 3 $k_3' \theta_{HCHO} = k_3 P_{HCHO}$
Step 4 $k_4 \theta_{HCHO} \theta_0^2 = k_4' \theta_{CO_2} \theta_{H_2O}$
Step 5 $k_5' \theta_{CO_2} = k_5 P_{CO_2}$
Step 6 $k_6' \theta_{H_2O} = k_6 P_{H_2O}$
Step 7 $\theta_{H_2O} = k_7 \theta_H^2 \theta_0$.

In the above expressions, k_i and k_i' are the adsorption and desorption rate constants for reaction Step i, except k_4, k_4', and k_7, which represent the surface reaction rate constants; θ is the surface coverage; and P is the partial pressure of the species in the reactor.

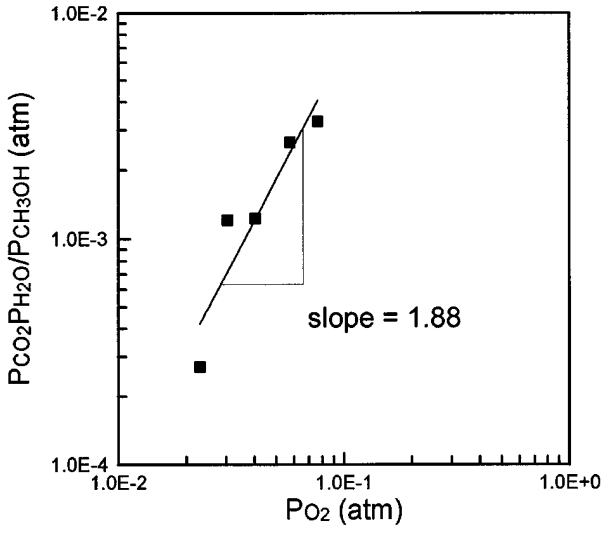

FIG. 6. Dependence of $P_{CO_2}P_{H_2O}/P_{CH_3OH}$ on P_{O_2}.

From Step 4, which is the supposed rate-limiting step, r_{0,CO_2} can be derived as

$$r_{0,CO_2} = k_4 \theta_{HCHO} \theta_0^2 - k_4' \theta_{CO_2} \theta_{H_2O}$$
$$= \frac{k_4 K_1^{1.5} K_2 k_7 P_{CH_3OH} P_{O_2}^{0.5}}{K_6 P_{H_2O}} - k_4' K_5 K_6 P_{CO_2} P_{H_2O}, \quad [20]$$

where K_i is k_i/k_i'. The last term for the above rate equation can be neglected for low conversion of CH_3OH. Because r_{0,CO_2} is nearly proportional to P_{CO_2} in the CSTR reactor for low conversion, $P_{CO_2}P_{H_2O}/P_{CH_3OH}$ must be proportional to $P_{O_2}^{1.5}$ from Eq. [20]. Figure 6 represents the relationship of both terms, $P_{CO_2}P_{H_2O}/P_{CH_3OH}$ and P_{O_2}, in logarithmic scale. The slope calculated by the least-squares method was found to be 1.88, which is seen to be close to the value of 1.5 predicted by the rate equation.

P_{HCHO} can also be written as

$$P_{HCHO} = \frac{\theta_{HCHO}}{K_3} = \frac{K_1^{0.5} K_2 k_7 P_{CH_3OH} P_{O_2}^{0.5}}{K_3 K_6 P_{H_2O}} \propto r_{0,HCHO}. \quad [21]$$

From the above Eq. [21], $P_{HCHO}P_{H_2O}/P_{CH_3OH}$ should be proportional to $P_{O_2}^{0.5}$. The logarithmic plot of both terms is shown in Fig. 7, where the slope calculated was found to be 0.20. Although this value is smaller than 0.5, predicted from the rate equation, the two values are not considered to differ greatly when we consider experimental errors and the many assumptions introduced in the mechanism and during the derivation of the rate equations. Therefore, the rate equations based on the reaction mechanism are seen to explain the experimental data fairly well, and will be used in the following section for the explanation of the NEMCA effect.

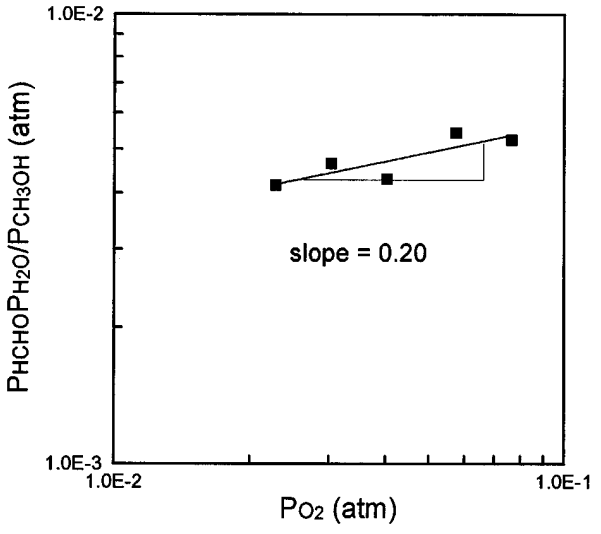

FIG. 7. Dependence of $P_{HCHO}P_{H_2O}/P_{CH_3OH}$ on P_{O_2}.

Effect of Cathodic Overpotential on CH_3OH Oxidation

The effect of the cathodic overpotentials on the rate of CH_3OH oxidation at steady state was investigated to see whether the NEMCA effect influenced the catalytic CH_3OH oxidation rate. As explained in the Introduction, the cathodic overpotential ($\Delta V_{WR} < 0$) corresponds to the O^{2-} ion pumping from the catalyst to the counter electrode and gives the cathodic current ($I < 0$). After the cathodic overpotential was applied by decreasing the catalyst potential below the OCP, the corresponding changes in catalytic oxidation rates in terms of $\Delta r_{CO_2(experimental)}$ and $\Delta r_{HCHO(experimental)}$ were measured by gas chromatography and mass spectroscopy, where $\Delta r_{CO_2(experimental)} = r_{CO_2} - r_{0,CO_2}$ and $\Delta r_{HCHO(experimental)} = r_{HCHO} - r_{0,HCHO}$. When the application of the catalyst potential change from its open circuit value was stopped, the catalytic oxidation rate returned to its original value. Therefore, the effect of the cathodic overpotential was found to be reversible.

Figure 8 shows such variation of r_{CO_2}, r_{HCHO}, and current with the cathodic overpotentials at a reaction temperature of 500°C, an inlet P_{O_2} of 0.05 atm, and an inlet P_{CH_3OH} of 0.05 atm. Little change was observed in r_{HCHO}, while r_{CO_2} increased steadily up to 0 cathodic overpotential of −500 mV and then increased slightly with the cathodic overpotential. $|I|$ is also seen to increase exponentially with the cathodic overpotential. The OCP, V°_{WR}, in this reaction condition was −735 mV, as shown in Table 1. This implies that electrochemical reactions such as Eqs. [15] and [16] are proceeding comparably with the oxygen exchange reaction. The current in Fig. 8 represents the sum of the current for each reaction proceeding on the Ag electrode and this relation can be written as

$$I = I_{O_2} + I_{HCHO} + I_{CO_2}, \qquad [22]$$

where I_{O_2}, I_{HCHO}, and I_{CO_2} are the current for the oxygen exchange reaction, reaction [15], and reaction [16], respectively. As the observed OCP was a mixed potential, equal amounts of cathodic current for the oxygen exchange reaction and anodic current for reactions [15] and [16] flow under the open circuit condition. Therefore, no apparent current flow is observed. Under the assumption that the oxygen coverage on the Ag electrode is not affected by the addition of CH_3OH to $He–O_2$ flow when conversion of CH_3OH is low (below 30%), it is reasonable that I_{O_2} is assumed to be the same as the limiting current (−0.3 mA) at the high-cathodic overpotential in $He–O_2$ flow which was discussed in Fig. 3. The sum of I_{HCHO} and I_{CO_2} is then calculated by the subtraction of I_{O_2} from I. At this stage, however, it is difficult to determine I_{HCHO} and I_{CO_2} separately because a distinct nonfaradaic reaction takes place when current flows, which will be stated below. As shown in Fig. 8, the change in the oxidation rate with the cathodic overpotential was distinct in r_{CO_2} and from this, the sum of I_{HCHO} and I_{CO_2} might be mainly attributed to the electrochemical oxidation of CH_3OH to CO_2. In such a case, I_{HCHO} is negligible and Eq. [22] is rewritten as follows:

$$I = I_{O_2} + I_{CO_2}. \qquad [23]$$

Since I_{O_2} is assumed to be known from the limiting current I_{CO_2} can be determined using Eq. [23] and is listed in Table 3. The faradaic oxidation rate of CH_3OH to CO_2($\Delta r_{CO_2(faradaic)}$) upon current flow, where oxidation is assumed to occur only through the net charge transfer reaction under Faraday's law, can be estimated by the following relation; which is based on reaction [16]:

$$\Delta r_{CO_2(faradaic)} = \frac{I_{CO_2}}{6F}. \qquad [24]$$

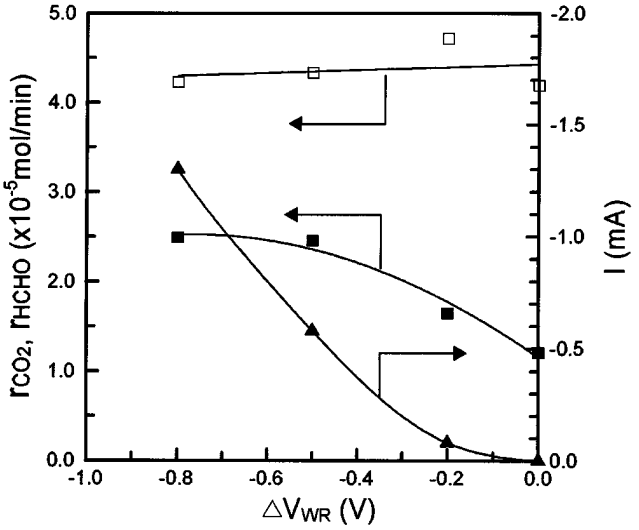

FIG. 8. Variation of r_{CO_2} (■), r_{HCHO} (□), and current (▲) with the cathodic overpotential. $T = 500$°C, inlet $P_{O_2} = 0.05$ atm, and inlet $P_{CH_3OH} = 0.05$ atm.

TABLE 3

Currents and Changes in Rates of Formation of CO_2 (Faradaically Calculated and Experimentally Obtained) at Various Cathodic Overpotentials

Cathodic overpotential (mV)	I (mA)	I_{O_2} (mA)	I_{CO_2} (mA)	$\Delta r_{CO_2(\text{faradaic})}$ ($\times 10^{-6}$ mol/min)	$\Delta r_{CO_2(\text{experimental})}$ ($\times 10^{-6}$ mol/min)
−200	−0.08	−0.30	0.22	0.02	4.4
−500	−0.58	−0.30	−0.28	−0.03	12.5
−800	−1.30	−0.30	−1.00	−0.10	12.8

The negative sign of $\Delta r_{CO_2(\text{faradaic})}$ means that there is a decrease in r_{CO_2} upon current flow.

In Table 3, $\Delta r_{CO_2(\text{faradaic})}$ was compared with the change in r_{CO_2} ($\Delta r_{CO_2(\text{experimental})}$ measured by gas chromatography upon the current flow. It is clearly seen from Table 3 that $\Delta r_{CO_2(\text{experimental})}$ is much higher than $\Delta r_{CO_2(\text{faradaic})}$. This result indicates that the steady state increase in the rate of CO_2 formation upon lowering of the catalyst potential fairly exceeds the rate of faradaic formation of CO_2. From this result, it can be suggested that the enhancement of r_{CO_2} with the cathodic overpotential could not be explained by a faradaic reaction alone, but there must be other enhancement effects such as a NEMCA effect. If we calculate the enhancement ratio ρ, defined as (3–7)

$$\rho = \frac{r}{r_0}, \qquad [25]$$

it turns out to be as high as 2.1 for the CO_2 formation rate. A more straightforward analysis for the increase in catalytic reaction rate has been made elsewhere (3–7, 25) using the enhancement factor Λ defined as

$$\Lambda_{HCHO} = \frac{\Delta r_{HCHO}}{I/2F} \qquad [26]$$

$$\Lambda_{CO_2} = \frac{\Delta r_{CO_2}}{I/6F}. \qquad [27]$$

As shown in Fig. 8, it is found that $\Lambda_{HCHO} = 0$ and $\Lambda_{CO_2} = -95.5$ for the cathodic overpotential of −0.8 V. The negative sign indicates that the reaction is electrophilic, or equivalently the rate is accelerated with decreasing catalyst work function (3–7, 25). As for the magnitude of Λ_{CO_2}, it is in agreement with those measured for CH_3OH decomposition on Ag (25) and for CH_3OH oxidation on Pt (7). From Eq. [5], r/r_0 is supposed to increase exponentially with the catalyst potential, or the overpotential, but Fig. 8 reveals that r/r_0 for the rate of CO_2 formation over Ag does not follow the relationship of Eq. [5]. Such a difference seems to appear because Eq. [5] is based on a first-order Eley–Rideal reaction model (5), whereas the reaction mechanism of CH_3OH oxidation over Ag is quite different.

As shown in Fig. 8, r_{CO_2} increased with the cathodic overpotential while r_{HCHO} remained unchanged. This result strongly implies that cathodic overpotentials had an influence on the rate constant of the limiting step, k_4, in terms of a nonfaradaic enhancement effect on the surface reaction between $HCHO_{(a)}$ and $O_{(a)}$. A decrease in the catalyst potential by applying cathodic overpotentials is supposed to have increased k_4, resulting in an increase in r_{CO_2}, because r_{0,CO_2} is proportional to k_4 from Eq. [20]. However, as $r_{0,\,HCHO}$ is not dependent on k_4, as seen in Eq. [21], little change in r_{HCHO} could be observed.

Variations of the CH_3OH oxidation rate with inlet P_{O_2} are shown in Figs. 9 and 10, respectively, where filled bars represent rates under open circuit conditions (r_{0,CO_2} $r_{0,HCHO}$) and open bars represent rates obtained when the cathodic overpotential of −500 mV was applied (r_{CO_2}, r_{HCHO}) at each inlet reactant composition. Numbers in parentheses represent current (mA) measured during the polarization r_{0,CO_2} and $r_{0,\,HCHO}$ at inlet P_{O_2} of 0 atm are seen to be considerably lower than those at P_{O_2} above 0.03 atm. From Fig. 9, if we compare the oxidation rate of CH_3OH to CO_2 between the open circuit condition and the cathodic polarization condition where a cathodic overpotential of −500 mV was applied at the given inlet P_{O_2}, it is found that the difference between r_{0,CO_2} and r_{CO_2} was negligible at P_{O_2} of 0 atm but it was distinct at P_{O_2} above 0.03 atm. The currents were, however, about the same for these P_{O_2}; i.e., the O^{2-} ions are diffusing on the Ag catalyst at the comparable rates for the various values of P_{O_2}. These results indicate that the enhancement of the CO_2 formation rate by the application

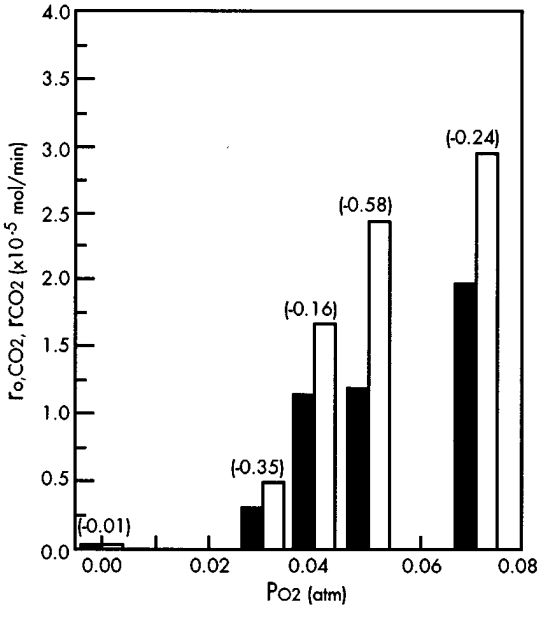

FIG. 9. Variation of r_{0,CO_2} and r_{CO_2} with inlet P_{O_2} under two different conditions: under open circuit condition (■) and at the cathodic overpotential of −500 mV (□). $T = 500°C$ and inlet $P_{CH_3OH} = 0.05$ atm.

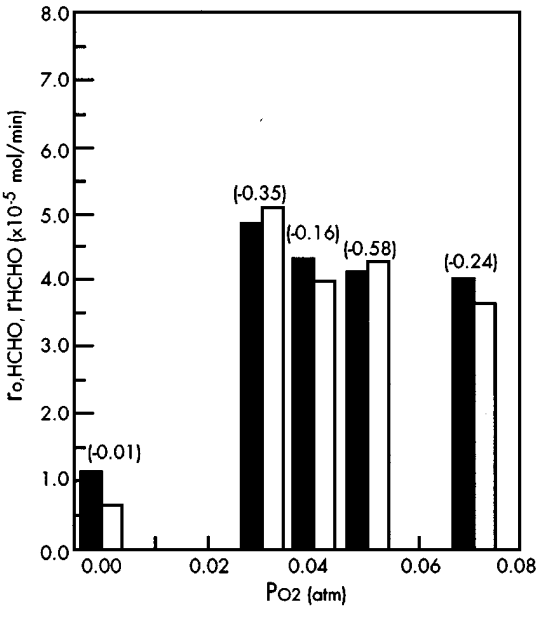

FIG. 10. Variation of $r_{0,\mathrm{HCHO}}$ and r_{HCHO} with inlet P_{O_2} under two different conditions; under open circuit condition (■) and at the cathodic overpotential of −500 mV (□). $T = 500°\mathrm{C}$ and inlet $P_{CH_3OH} = 0.05$ atm.

of the cathodic overpotential might not be directly due to the O^{2-} ions on the catalyst.

Although a distinct increase in the CO_2 formation rate was observed with the decrease in the catalyst potential at P_{O_2} above 0.03 atm, as is seen from Fig. 10, little change was observed even if P_{O_2} increased up to 0.07 atm for the HCHO formation rate. This phenomenon can be explained through the reaction mechanism and rate equations. Because $r_{O,\,CO_2}$ is proportional to k_4 and $P_{O_2(g)}^{1.5}$ from Eq. [20], an increase in r_{CO_2} with decrease in the catalyst potential at high P_{O_2} was evident, as shown in Fig. 9. But, for r_{HCHO}, where $r_{0,\,\mathrm{HCHO}}$ appears to be proportional to $P_{O_2(g)}^{0.5}$, changes were not evident, as shown in Fig. 10. It can be concluded from thse results that the enhancement of the CO_2 formation rate was due to an increased reaction rate between adsorbed oxygen and adsorbed HCHO, thereby increasing k_4.

The change in r_{CO_2} with cathodic overpotential can be explained qualitatively in terms of the NEMCA effect. When the cathodic overpotential is applied in such a way that $\Delta V_{WR} < 0$, O^{2-} ions are removed from the catalyst to the counter electrode through an electrolyte, and there is a decrease in the catalyst work function. A decrease in the catalyst potential causes an increase in the metal–electron acceptor adsorbate bond strength and a weakening in the intraadsorbate bonds as well. This has been already shown to drastically promote both the dehydrogenation and decomposition rates (25) in the case of CH_3OH dehydrogenation and decomposition on Ag and in the case of CH_3OH oxidation on Pt(7). Therefore, it is expected that even if Ag–O and Ag–HCHO bonds are strengthened with decreasing catalyst potential, a loosening in the intraadsorbate bonds of HCHO activates the decomposition of adsorbed HCHO, leading to an increase in the rate constant of the limiting step in CH_3OH oxidation, k_4, and thereby promoting the overall rate of CO_2 formation, r_{CO_2}.

CONCLUSIONS

The O_2 exchange reaction and the electrochemical oxidation of CH_3OH were carried out over a Ag electrode, about 10 μm in thickness, which was deposited by a screen printing method on a YSZ disk. From the O_2 exchange reaction in He–O_2 flow, the OCP and current–overpotential curves were reversibly obtained and it was found that oxygen adsorbed on Ag was in thermodynamic equilibrium with that in the gas phase. It was also seen that the cathodic limiting current was proportional to $P_{O_2}^{0.5}$ and resulted from the interfacial diffusion of adsorbed oxygen to the electrode–electrolyte–gas three-phase boundary where charge transfer took place. When CH_3OH was mixed into the He–O_2 flow, the OCP showed a value lower by several hundred millivolts than that in He–O_2 flow. This lowered OCP could be explained by a mixed potential which resulted from the kinetic equilibrium of the electrochemical reactions between CH_3OH and O_2.

Under open circuit conditions, a steady increase in r_{0,CO_2} was observed with the increase in inlet P_{O_2} and from this, oxidation of adsorbed HCHO was presumed to be a rate-limiting step. Rate equations were based on the reaction mechanism already reported in the literature and were found to be in good agreement with the experimental data analysis. By applying a cathodic overpotential, an enhancement of r_{CO_2} which fairly exceeds the faradaic formation rate of CO_2 was evident at P_{O_2} above 0.03 atm. From the proposed rate equations and changes in catalytic oxidation rates with the cathodic overpotentials, it was concluded that a decrease in the catalyst potential caused a weakening in the intraadsorbate bond strengths and a concomitant nonfaradaic enhancement of r_{CO_2}.

REFERENCES

1. Sawyer, D. T., and Roberts, J. L., "Experimental Electrochemistry for Chemists," p. 3. Wiley, New York, 1974.
2. Vetter, K. J., "Electrochemical Kinetics," p. 9. Academic Press, New York, 1967.
3. Vayenas, C. G., Bebelis, S., and Kyriazis, C. G., *Chem. Tech. Aug.*, 500 (1991).
4. Vayenas, C. G., Bebelis, S., and Ladas, S., *Nature* **343**, 15 (1990).
5. Vayenas, C. G., Bebelis, S., and Neophytides, S., *J. Phys. Chem.* **92**, 5083 (1988).
6. Ladas, S., Kennou, S., Bebelis, S., and Vayenas, C. G., *J. Phys. Chem.* **97**, 8845 (1993).
7. Vayenas, C. G., and Neophytides, S., *J. Catal.* **127**, 645 (1991).
8. Satterfield, C. N., "Heterogeneous Catalysis is Practice," p. 196. McGraw–Hill, New York, 1980.
9. Xinhe, B., Jingfa, D., and Shuzhong, D., *Surf. Sci.* **163**, 444 (1985).
10. Xinhe, B., and Jingfa, D., *J. Catal.* **99**, 391 (1986).

11. Jede, R., Manske, E., An, L. D., Ganschow, O., Kaiser, U., Wiedmann, L., and Benninghoven, A., *in* "Proceedings, 8th International Congress in Catalysis, Berlin, 1984," Vol. 2, p. 521. DECHEMA, Frankfurt, 1984.
12. Robb, D. A., and Harriot, P., *J. Catal.* **35**, 176 (1974).
13. Bhattacharyya, S. K., Nag, N. K., and Ganguly, N. D., *J. Catal.* **23**, 158 (1971).
14. Hong, J. K., Oh, I.-H., Hong, S.-H., and Lee, W. Y., *Appl. Surf. Sci.* **89**, 229 (1995).
15. Parthasarathy, A., Srinivasan, S., Appleby, A. J., and Martin, C. R., *J. Electrochem. Soc.* **139**, 2856 (1992).
16. Sheldon, B. W., "SOLGASMIX-PV For the PC." Oak Ridge National Lab., Oak Ridge, TN, 1989.
17. Barin, I., and Knacke, O., "Thermochemical Properties of Inorganic Substances." Springer-Verlag, Berlin/Dusseldorf, 1973.
18. Hillary, A., and Stoukides, M., *J. Catal.* **113**, 295 (1988).
19. Bard, A. J., and Faulkner, L. R., "Electrochemical Methods," p. 103, Wiley, New York, 1980.
20. Wang, D. Y., and Nowick, A. S., *J. Electrochem. Soc.* **126**, 1155 (1979).
21. Wang, D. Y., and Nowick, A. S., *J. Electrochem. Soc.* **128**, 55 (1981).
22. Vayenas, C. G., *J. Catal.* **90**, 371 (1984).
23. Otsuka, K., *Shokubai* **36**, 10 (1994).
24. Gopel, W., Hesse, J., and Zemel, J. N., "Sensors," Vol. II. p. 171. VCH Verlagsgesellschaft, Weinheim, 1991.
25. Neophytides, S., and Vayenas, C. G., *J. Catal.* **118**, 147 (1989).
26. Wachs, I. E., and Madix, R. J., *Surf. Sci.* **76**, 531 (1978).
27. Xinhe, B., and Jingfa, D., *Catal. Lett.* **4**, 25 (1990).